NeuroImage: Clinical 45 (2025) 103761

Contents lists available at ScienceDirect

NeuroImage: Clinical

journal homepage: www.elsevier.com/locate/ynicl

Hypoperfusion regions linked to National Institutes of Health Stroke Scale scores in acute stroke

Hana Kim [a,1], Alex Teghipco [b,1], Chris Rorden [b], Julius Fridriksson [c], Mathew Chaves [d], Argye E. Hillis [d,*]

[a] Department of Communication Sciences & Disorders, University of South Florida, USA
[b] Department of Psychology, University of South Carolina, USA
[c] Department of Communication Sciences & Disorders, University of South Carolina USA
[d] Departments of Neurology and Physical Medicine & Rehabilitation, Johns Hopkins School of Medicine, USA

ARTICLE INFO

Keywords:
CT
Perfusion
Acute Ischemic Stroke
NIHSS
Brain mapping

ABSTRACT

Background: The National Institutes of Health Stroke Scale (NIHSS) is widely used to assess stroke severity. While prior studies have identified subcortical regions where infarcts correlate with NIHSS scores, stroke symptoms can also arise from hypoperfusion, not just infarcts. Understanding the potential for neurological recovery post-reperfusion is essential for guiding treatment decisions. The goal of this study was to identify brain regions where hypoperfusion correlates with NIHSS scores, using computed tomography perfusion (CTP) scans in cases of acute ischemic stroke.

Methods: In this prospective observational study, we analyzed CTP scans and NIHSS scores from 89 patients in the acute phase. We employed a unique support vector regression approach to overcome limitations of traditional mass univariate analyses. Additionally, we used stability selection to identify the most consistent features across subsets, reducing overfitting and ensuring robust predictive models. We verified the consistency of results through nested cross-validation.

Results: Both cortical and subcortical areas, including white matter tracts, showed associations with NIHSS scores. These regions aligned with functions such as language, spatial attention, sensory, and motor skills, all assessed by the NIHSS.

Conclusions: Our findings reveal that hypoperfusion in specific brain regions, including previously underreported cortical areas, contributes to NIHSS scores in acute stroke. Moreover, this study introduces a novel brain mapping approach using CTP imaging and stability selection, offering a more comprehensive view of acute stroke impairments and the potential for recovery before structural reorganization occurs.

1. Introduction

The National Institutes of Health Stroke Scale (NIHSS) is a widely used tool for quantifying stroke severity. Several research teams have investigated the brain regions most associated with functional deficits in acute stroke, as measured by the NIHSS (Lyden et al., 1999). These studies used acute magnetic resonance imaging (MRI) diffusion-weighted images (DWI) to identify infarct locations and used various statistical approaches to determine the voxels most strongly associated with NIHSS scores. An early study created a three-dimensional atlas depicting the locations of lesions that contributed to the NIHSS score, demonstrating that lesion location, rather than lesion volume alone, was a better predictor of stroke severity (Menezes et al., 2007). This study found that voxels where lesions contributed most to NIHSS scores were located in bilateral subcortical areas (Menezes et al., 2007). Other studies have identified small clusters of voxels in subcortical regions and white matter tracts (Rajashekar et al., 2022), as well as the bilateral caudate and insula (Zavaglia et al., 2015), as areas where acute lesions had the most impact on the NIHSS score. Another study showed how structural or functional disconnections caused by lesions contributed to NIHSS scores (Ding et al., 2023).

Despite the large sample sizes and sound methodologies, these

* Corresponding author at: Physical Medicine & Rehabilitation, and Cognitive Science, Johns Hopkins University School of Medicine, Baltimore, MD 21287, USA.
E-mail address: argye@jhmi.edu (A.E. Hillis).
[1] These authors contributed equally.

https://doi.org/10.1016/j.nicl.2025.103761
Received 25 October 2024; Received in revised form 12 February 2025; Accepted 17 February 2025
Available online 21 February 2025

studies produced highly heterogeneous results, with few consistent findings regarding the specific lesion locations most closely linked to NIHSS scores. Remarkably, all of the studies identified predominantly subcortical voxels and structures. Although it is expected that some subcortical regions, such as the internal capsule and other parts of the corticospinal tract, are crucial for motor functions measured by the NIHSS, it is surprising that few cortical areas were identified as critical. Given that the NIHSS assesses language, orientation, vision, and spatial attention—functions typically associated with cortical regions—this discrepancy remains puzzling.

The main limitation of previous approaches is their narrow focus on core infarcts visible on DWI, overlooking the role of surrounding hypoperfused tissue. Functional deficits in acute stroke often result not only from the infarct but also from the surrounding area of the penumbra—an area of tissue that receives enough blood to survive but not enough to function properly (Olsen et al., 1983). Ample studies have demonstrated that language deficits, for example, are more strongly related to the entire area of dysfunctional tissue, including both the infarct and the region of cortical hypoperfusion (Croquelois et al., 2003; Hillis et al., 2002; Hillis et al., 2006; Ochfeld et al., 2010). Furthermore, current acute stroke studies often rely on computed tomography perfusion (CTP), rather than DWI and MRI perfusion scans, to guide clinical management. While software packages (e.g., RAPID AI) readily yield maps that display voxels exceeding a given threshold of hemodynamic measures (e.g., Tmax > 5), the maps use opaque formats, making it challenging to analyze granular perfusion data.

Identifying the brain regions where hypoperfusion contributes most to the severity of functional deficits is critical for the clinical management of acute ischemic stroke. Optimally, clinicians need to inform patients and their caregivers about the potential for recovery if acute treatments (e.g., thrombectomy) successfully reperfuse the ischemic penumbra. Subcortical areas often infarct early and may not regain function even with restored blood flow, but cortical areas may be salvageable. Therefore, it is important to understand which regions are most likely to recover after reperfusion. Our study aimed to answer the question: Which brain regions, when hypoperfused, have the greatest impact on neurological function as reflected in the NIHSS? We hypothesized that the regions contributing to the NIHSS score would include more cortical areas than previously identified, along with subcortical structures and white matter tracts.

In summary, our study addressed two critical gaps in previous research. First, while prior studies focused on DWI to identify areas of permanent damage, they overlooked the broader scope of functional disruptions caused by hypoperfusion. By leveraging acute CTP imaging, we captured the full extent of transient disruptions, which may offer more actionable insights for clinical decision-making. Second, we utilized an advanced machine learning method—stability selection—to avoid the common pitfall of overfitting in smaller datasets. This approach ensured that our model identified the most consistent and relevant brain regions associated with NIHSS scores, providing a robust framework for predicting functional deficits in acute stroke. These innovations enabled us to reveal critical cortical and subcortical areas involved in stroke impairments..

2. Methods

2.1. Participants

This study included 89 individuals with acute ischemic stroke (38 women, mean age = 63.2 years, standard deviation [SD] = 13.5 years). Demographics are shown in Table 1. This cohort reflects a consecutive series of individuals who met the inclusion criteria and were identified from a larger prospective study investigating diverse aspects of behavioral performance following acute ischemic stroke, based on having undergone a CTP scan acutely. All participants, or their legally authorized representatives, provided informed consent in compliance with the Declaration of Helsinki. Exclusion criteria included: a) lack of premorbid fluency in English; b) uncorrected vision or hearing impairments; c) any conditions or circumstances that hindered their involvement in the testing procedures (such as reduced levels of consciousness or being intubated); and d) a documented history of dementia or other neurological disorders that impacted brain function. These last conditions were identified by self or family report or documentation in the medical records.

Table 1
Demographics.

Variable*	Mean (SD) Or Number
Age	63.2 (13.5)
Sex (F/M)	38/51
Hemisphere of stroke (Right/Left)	42/47
Time between onset of stroke symptoms and CTP scan (minutes)	656 (655)
NIHSS score	11.4 (6.8)Range: 1–27 Median:11
Treatment (following assessment)	
Medical only (N)	45
Intravenous thrombolysis only (N)	18
Endovascular only (N)	14
Thrombolysis + Endovascular (N)	12
Location of clot (if seen on imaging)	
Internal carotid artery	8 L, 8 R
Middle cerebral artery (MCA)	5 LM1, 9 LM2, 11 RM1, 8 RM2
Anterior cerebral artery (ACA)	1 LA1, 1LA2, 1 RA1, 0RA2
Posterior cerebral artery (PCA)	2 LP1, 1LP2, 2 RP1, 1 RP2
Basilar artery	3

Abbreviations: N = number, L = left, R = right, M1 = MCA first segment, M2 = MCA second segment (branch); A1 = ACA first segment, A2 = ACA second segment; P1= PCA first segment, P2 = PCA second segment.

Patients with strokes primarily in the brainstem or cerebellum were also excluded. The study and the consent forms were approved by the Johns Hopkins University (JHU) Institutional Review Board (approval number: NA_00042097).

2.2. Behavioral measures

In nearly all cases, NIHSS scores were recorded within 30 min of arrival in the emergency department by a neurology resident or stroke attending, about the same time as the CTP scan. When the CTP and NIHSS assessments were conducted outside of the emergency department (e.g., strokes that occurred in the hospital), an experienced stroke neurologist conducted a thorough chart review to calculate the NIHSS score within one hour of the CTP (Williams et al., 2000). When the patient received intravenous thrombolysis or endovascular therapy, both the CTP and NIHSS scores used in this study were recorded before the intervention.

2.3. Imaging data and preprocessing

CT imaging was conducted on a Siemens Somatom Drive (Siemens, Erlangen, Germany), with dimensions of 512x512x49 voxels and 0.4x0.4x3 mm resolution. Using a pre-specific protocol, patients received a 50 ml injection of non-ionic iodinated contrast material followed by 30 ml saline, delivered at a rate of 5–6 ml per second. Slice thickness was 5 mm. The scanning parameters were as follows: 70 kVP, 200 mAs, with a rotation time of 0.25 seconds. Average acquisition time was 60 seconds. The collimation used was 48 x 1.2 mm, with a pitch value of 0.7, and a 4D coverage range of 114 mm at an interval of 1.5 seconds, scanning in a craniocaudal direction. Following the acquisition, perfusion images were postprocessed with RAPID CT (RapidAI, Menlo Park, CA, United States), resulting in proprietary red–green–blue images measuring 256 × 286 × 15 voxels at 0.8x0.8x10 mm, capturing multiple perfusion measures: quantitative volumes for relative cerebral blood

flow (CBF), cerebral blood volume (CBV), mean time to transit (MTT), and time to maximum of residue function (Tmax). The degree of hypoperfusion for the current paper was defined as the number of seconds delay in Tmax (see results for rationale). Initially, the signal-to-noise ratio of the structural CT data was enhanced by creating a mean structural image. The structural data were deskulled without applying any smoothing or thresholding. When necessary, adjustments were made to optimize brain extraction. Structural and perfusion images were aligned and then normalized to a CT template. Deformation was applied to align the JHU-MNI atlas with participant anatomy. Finally, participant-level perfusion maps were mean-scaled, and regional perfusion measures from 189 grey and white matter regions of the JHU-MNI atlas were extracted by averaging voxel values.

2.4. Statistical analysis

Multivariate machine learning can map more complex brain-deficit relationships than the more commonly used mass univariate methods, which treat each voxel independently (Mah et al., 2014). However, when faced with numerous features (e.g., brain regions), substantial noise (e.g., many features irrelevant to stroke severity), and high feature similarity (e.g., topographic bias of lesions), these methods can favor overly simple models that benefit generalizability (Zou and Hastie, 2005; Mwangi et al., 2014; Hastie et al., 2009). Mechanisms for mitigating overfitting help models navigate such challenging landscapes, but they can also destabilize model performance and learned patterns of feature importance, compromising model interpretability (Zou and Hastie, 2005; Mwangi et al., 2014; Meinshausen and Bühlmann, 2010; Hardin et al., 2004).

Here, we implemented a pipeline that we recently showed can reveal more robust multivariate brain-deficit associations in similar sample sizes (Teghipco et al., 2024; Teghipco et al.). Our key innovation is the identification of *reliably* predictive brain regions that help stabilize models and their learned feature weights, thereby improving prediction accuracy (Teghipco et al., 2024). In this pipeline, we identified predictive regions across various model specifications and perturbed training datasets. A more sophisticated model then refined the importance of these regions, directing the model's limited capacity to extract more meaningful signals from the data. For comprehensive methodological details, we refer the reader to our prior work (Teghipco et al., 2024).

Nested cross-validation (CV) was used to train and test models predicting NIHSS. Leave-one-out CV was applied in the outer folds for testing, while an inner 8-fold CV tuned a support vector regression (SVR) model. Stability selection with elastic net identified stable features in the outer training data by drawing 200 random subsamples of 75 participants. Elastic net models were applied to each subsample using 1,000 log-spaced λ values (ranging from 0 to the maximum value with a non-null model) and 21 linearly spaced α values between 0 and 1. We tracked the first 30 of 756 features (189 regions of interest [ROIs] for four perfusion measures) entering each model and calculated the empirical selection probability as the highest proportion of subsamples in which a feature was chosen. The stable feature set was defined by the probability threshold that limited the number of false positives to 0.05. A nonlinear SVR was tuned using stable features, with Bayesian optimization (100 evaluations) adjusting three key hyperparameters (default ranges in MATLAB's Statistics and Machine Learning Toolbox): ϵ (error tolerance), C (margin deviations), and γ (Gaussian kernel radius).

We repeated nested CV 20 times to produce more robust point estimates of model performance. The Pearson correlation coefficient determined whether model predictions explained a significant amount of variance in NIHSS scores. Additionally, a naïve model was used to predict NIHSS scores based on the training set mean. The mean absolute error (MAE) of the true model was scaled to the MAE of this naïve model (MASE) and expressed as a percentage to capture prediction accuracy: $100\times(1 - \text{MASE})$. (Franses, 2016).

We performed the repeated nested CV without stability selection to confirm its beneficial impact on the model. Additionally, we tested whether adding demographic variables (age, sex, education, and time between stroke and scan) after stability selection positively affected model performance.

The nonlinear SVM refined feature importance among stable features. We evaluated importance using Shapley Additive Explanations (SHAP), which captured the extent to which a feature deviated the model's predictions from the average or baseline prediction. A formulation of Kernel SHAP was used that estimates conditional expectations through k-nearest neighbors sampling (10 % of samples), taking into account feature dependencies (Aas et al., 2021). Absolute SHAP values were generated for each model in the repeated nested CV scheme and averaged to produce one value per feature. We z-scored these values, determining that features below 2.1 (approximately corresponding to $p > 0.05$) had lesser contributions to predictions in the group.

2.5. Data sharing and availability

We provide open-source software to replicate and reuse the processing stages developed in this study (https://github.com/alexteghipco/CTPerfusionPipeline). Additionally, anonymized data will be made available upon request to the authors, subject to review by the JHU Institutional Review Board, resulting in a formal data sharing agreement.

3. Results

The average time interval between the onset of stroke symptoms (or last known well) and CT acquisition was approximately 10 hours and 9 minutes. Both NIHSS and CT exams were done before any treatment. See Table 1 for additional information on location of clots and subsequent treatment.

SVR models trained on reliably predictive features (brain regions or ROIs) identified through stability selection generated predictions that explained a significant amount of variance in true NIHSS scores across all 20 CV repeats (the highest p-value was 0.00000004). Additionally, these models consistently demonstrated at least 20 % higher accuracy, based on mean absolute error, than naïve guessing (i.e., accuracy percentage).

Consistent with our previous work, we found that selecting reliably predictive features enhanced model performance, resulting in higher prediction accuracy compared to using the full set of features (Fig. 1). Paired t-tests revealed that using all features resulted in significantly lower prediction accuracy, $t(19) = -14$, $p < 0.000001$, and weaker correlations with true NIHSS scores, $t(19) = -22$, $p < 0.000001$, across CV repeats. Furthermore, incorporating demographic variables alongside stable brain features produced a small but statistically significant 1 % improvement in prediction accuracy, $t(19) = 3.4$, $p = 0.003$ (Fig. 1).

We identified 44 features—representing roughly 6 % of the entire feature space—that were reliably predictive across datasets, appearing in at least 50 % of CV folds (Table 2). In describing the features driving the models, we focused on Tmax, as it is the map most commonly used to identify penumbral tissue clinically (Christensen et al., 2021) and exhibited the strongest predictive value. While our approach demonstrated the stability of CBF, CBV, and MTT (i.e., all modalities contributed to our models), we found that Tmax of brain regions drove predictions most strongly. Table 3 presents average feature z-scores for each perfusion measure (i.e., aggregated across all 189 ROIs), indicating that Tmax is the only CTP measure with a positive mean z-score. We further verified that brain regions with Tmax < 6 drove predictions toward less severe scores, while regions with Tmax > 6 drove predictions toward more severe scores. A Mann–Whitney U test on the directional SHAP values for these two groups of features confirmed this significant result ($p = 0.000001$).

Among the 189 ROIs examined, 21 showed a significant association between the degree of hypoperfusion (Tmax) and the NIHSS score.

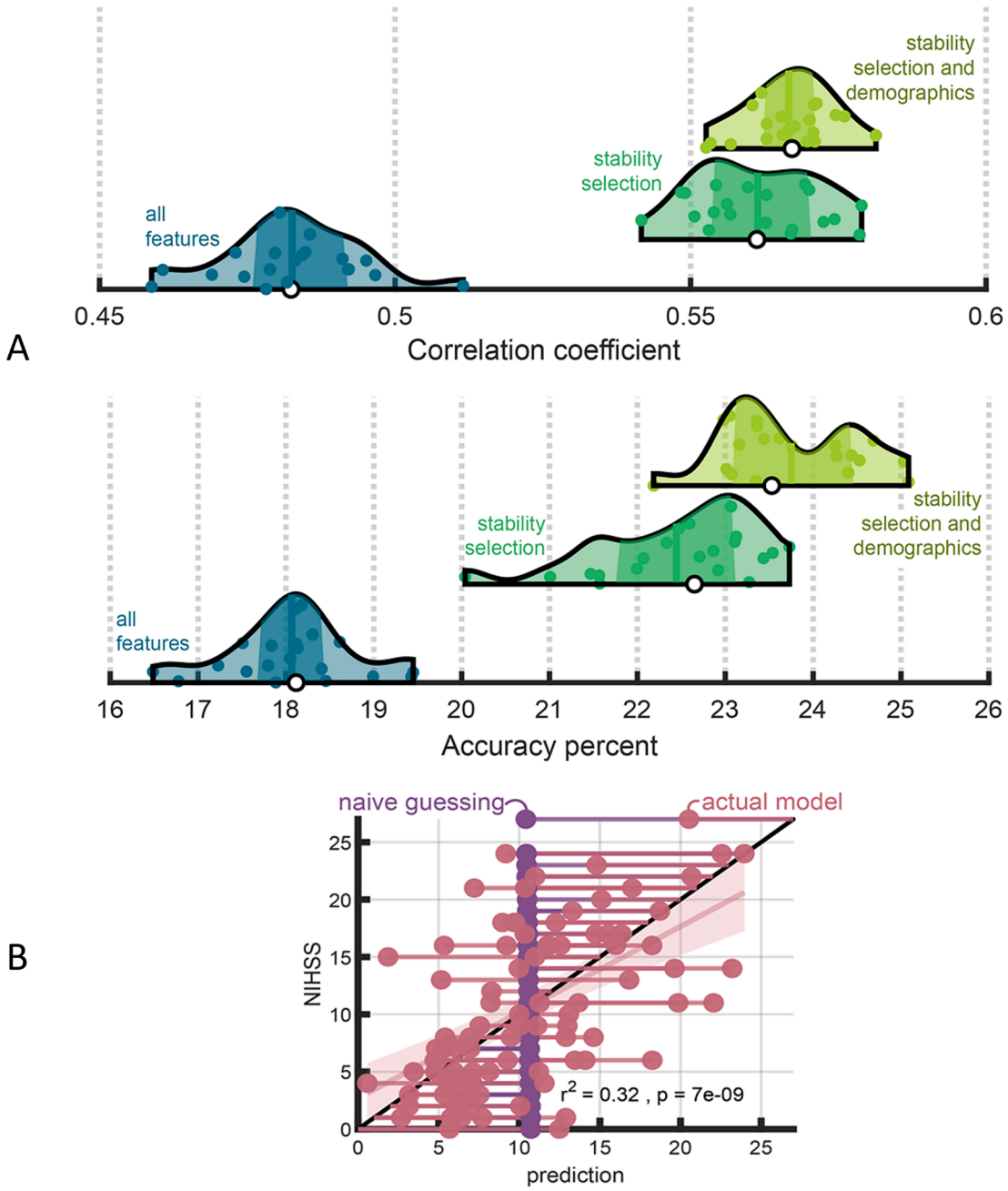

Fig. 1. Model performance in predicting NIHSS scores across repeated nested cross-validation. The accuracy percentage (x-axis) indicates model prediction accuracy relative to a naïve guessing model. For example, an accuracy percentage of 20 indicates that the model's predictions had a mean absolute error that was 20% lower than a model guessing based on the mean NIHSS of the training data. The accuracy percentage is shown for models trained on all features (blue), reliably predictive features identified by stability selection (green), and reliably predictive features combined with demographics (green-yellow). Each violin plot displays the distribution of model performance over 20 repeats of nested cross-validation. Colored dots inside each violin represent the results of a single repeat. The darker shaded area corresponds to the interquartile range, the white dot represents the median, and the colored vertical line corresponds to the mean.

Table 2 lists the ROIs identified by stability selection, using Tmax. Most ROIs were not selected; however, the majority of selected ROIs appeared consistently across most training datasets. Fig. 2 illustrates the ROIs where perfusion abnormalities (Tmax) correlated most strongly with NIHSS scores.

Given our relatively small participant pool, we also report the ROIs selected by stability selection in 1–50 folds (of 89 folds), as these may have shown significance with a larger number of participants (Table 4).

4. Discussion

This study focused on identifying specific brain regions where hypoperfusion is associated with NIHSS scores in acute ischemic stroke patients, using CTP scans to reveal these associations. While previous studies predominantly examined areas of infarct contributing to NIHSS scores by analyzing each voxel independently—leading to the identification of scattered clusters of voxels primarily in subcortical areas—our approach differed by targeting areas of hypoperfusion (i.e., delayed Tmax on CTP).

Previous research has evaluated the association of acute lesions with

Table 2
Features (ROIs) where hypoperfusion measured by Tmax was significantly associated with the NIHSS (in 50–99 folds).

ROI	Z-score
LH posterior insula	5.28
LH superior temporal gyrus	4.46
LH supramarginal gyrus	4.35
LH inferior frontal gyrus pars opercularis	4.20
LH insular cortex	4.14
LH posterior superior temporal gyrus	4.12
LH inferior frontal gyrus pars orbitals	4.11
LH inferior frontal gyrus pars triangularis	3.20
LH pole of superior temporal gyrus	3.18
LH posterior middle temporal gyrus	3.05
LH middle temporal gyrus	2.88
RH posterior superior temporal gyrus	5.30
RH supramarginal gyrus	4.75
RH superior temporal gyrus	4.24
RH uncinate fasciculus	3.80
RH pole of superior temporal gyrus	3.68
RH mammillary body	3.04
RH Inferior fronto-occipital fasciculus	2.99
RH external capsule	2.93
RH postcentral gyrus	2.90
RH lateral ventricle atrium	2.65

Tmax = time-to-maximum; LH = left hemisphere; RH = right hemisphere.

Table 3
CTP measure-specific average feature importance z-score.

CTP measure	Mean (Z-score)	Standard Error of the Mean (Z-score)
CBF	−0.137	0.04197
CBV	−0.0915	0.05566
MTT	−0.0781	0.06285
Tmax	0.20551	0.09432

scores on specific or functionally related items. One study found that language deficits were associated with small clusters of voxels in the middle temporal gyrus, superior temporal sulcus, and precentral gyrus (Cheng et al., 2023). Another study reported that language deficits measured by the NIHSS score were linked to tiny clusters of voxels in the left internal capsule, Heschl's gyrus, corticospinal tract, and subcortical Rolandic operculum (Rajashekar et al., 2022). The heterogeneity of these results may indicate that areas of hypoperfusion (not identified in these studies), rather than infarct areas, are responsible for language deficits in acute stroke.

Unlike these previous studies, we identified numerous cortical areas, as well as subcortical structures and white matter tracts, that contributed to the NIHSS score. The cortical regions where hypoperfusion consistently related to higher NIHSS scores included areas critical for language processing, such as the left supramarginal gyrus (SMG), posterior superior temporal gyrus, insula, middle temporal gyrus, temporal pole, and inferior frontal gyrus (pars opercularis, pars orbitalis, and pars triangularis). The areas with the strongest and most stable associations with NIHSS scores also included regions frequently associated with spatial attention (e.g., hemispatial neglect and extinction), such as right STG and SMG, and postcentral gyrus, critical for tactile sensation. We also identified white matter tracts commonly implicated in spatial attention networks, including right uncinate and inferior frontal occipital fasciculus.

Our analysis further identified motor areas where hypoperfusion correlated with NIHSS scores in 1 to 50 folds of the analysis. These areas included the posterior limb of the internal capsule (critical for limb strength) and the genu of the internal capsule (facial strength and speech articulation). The right anterior limb of the internal capsule, important for sensation and cognition, was also identified. Other areas identified as contributing to NIHSS in 1–50 folds of the analysis included additional language-related white matter tracts, such as the left superior longitudinal fasciculus (synonymous with the arcuate fasciculus in the JHU-MNI atlas), the left genu of the corpus callosum, and the left uncinate, as well as the right superior occipital gyrus, which is important for visual fields (another item on the NIHSS).

Some areas that contribute to the NIHSS score were not identified in this analysis, such as the left angular gyrus and thalamus (involved in language), bilateral thalami (involved in sensation, memory, and spatial attention), the left posterior limb of the internal capsule (involved in limb strength), the left superior occipital gyrus (involved in vision), and the cerebellum (critical for coordination). However, some areas may have been missed due to low statistical power; the number of participants with damage to each area may have been insufficient to capture all critical areas. Alternatively, while these regions may be necessary for complex language, cognitive, and motor tasks, residual processing may suffice for the NIHSS.

We chose to use Tmax, one of several hemodynamic maps generated by CTP RAPID AI software. Tmax is most frequently used to identify areas of hypoperfusion beyond the infarct that represent penumbral tissue, and it most strongly drove predictions toward higher NIHSS scores. However, we could have selected other hemodynamic measures. Note that we did not differentiate between "core/infarct" and penumbra for this analysis, as our goal was to identify the entire area of dysfunctional tissue contributing to deficits measured by the NIHSS. Studies have shown that Tmax > 6 indicates risk of progression to infarct, and Tmax > 10 likely indicates irreversible damage (strongly correlating with final infarct) (Wang et al., 2023). Our algorithm evaluated Tmax as a continuous measure since previous studies have demonstrated that greater delays in contrast correlate with worse dysfunction (Hillis et al., 2001).

The main limitation of the current study is the relatively low number of participants (n = 89) for a brain mapping study, which restricted our ability to identify all areas where dysfunction contributes to the NIHSS, and the restriction of participants to those with hemispheric strokes (excluding those with strokes limited to the brainstem or cerebellum). We also did not attempt to identify which areas are associated with different items on the NIHSS because this was beyond the scope of our study. However, we have identified specific functions associated with distinct areas of hypoperfusion in previous studies (Hillis et al., 2005; Hillis et al., 2004; Hillis et al., 2003; Hillis et al., 2001). Finally, we may have missed some areas of neuronal loss that can only be seen with higher resolution (e.g. 7 Tesla MRI).

Despite these limitations, this study provides clinically important and novel information about the relationship between hypoperfused brain tissue and NIHSS scores, enhancing our understanding of how specific brain regions contribute to deficits measured by the NIHSS. These findings can help clinicians predict functional recovery based on the salvageability of the penumbra and anticipate how NIHSS scores might improve with successful reperfusion. Although most trials have focused on the volume of penumbral tissue, the location also provides useful prognostic information (Menezes et al., 2007). Importantly, our study also illustrates a robust approach to using CTP for mapping brain functions, which can be applied to more finely evaluated functions than stroke severity measured by the NIHSS. Mapping lesion-deficit associations in the acute stage of stroke captures relationships before reorganization or recovery of function. However, the "lesion" must include areas of dysfunctional tissue identified with perfusion imaging, as acute deficits reflect both hypoperfusion and infarct.

Funding Statement

This work is supported by the National Institute on Deafness and Other Communication Disorders (NIDCD) through grants RF1-MH133701 (CR), R01 DC05375 (AEH, HK), R01 DC015466 (AEH), and P50 DC014664 (CR, JF, AEH).

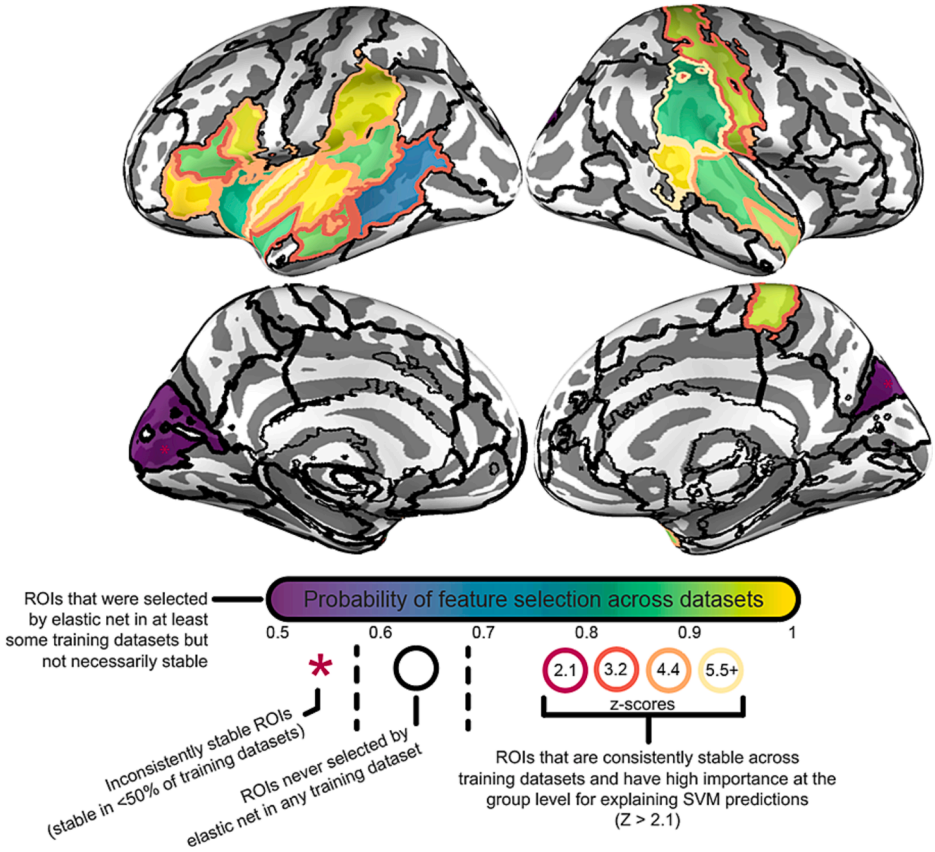

Fig. 2. Visualization of stable features that were highly influential in SVR model predictions. Each cortical feature (i.e., ROI) is depicted on a surface template by an outline. Black outlines with no solid color filling indicate features that were never selected across any subsamples in any training dataset. The median empirical probability of a feature being selected across all training datasets is shown in solid colors, representing the information used to determine whether a feature entered the stable set. Features that did not consistently enter the stable set (i.e., in at least half of the training datasets) are marked with a superimposed red asterisk. Colored outlines indicate features that were highly influential for predictions across all training datasets, with a SHAP value 2.1 SD above the average feature (after collapsing SHAP values across training datasets and cross-validation repeats). Higher z-scores for the SHAP values of features are denoted by brighter colored outlines.

Table 4
ROIs where hypoperfusion measured by Tmax was associated with the NIHSS score in 1–50 folds.

Left hemisphere	Right hemisphere
Uncinate	Retrolenticular limb of the internal capsule
Superior Longitudinal Fasciculus	Posterior limb of the internal capsule
Genu of the corpus callosum	Anterior limb of the internal capsule
Superior cerebellar peduncle	Superior cerebellar peduncle
Cuneus	Global pallidus
	Putamen
	Caudate

CRediT authorship contribution statement

Hana Kim: Writing – original draft, Investigation, Data curation. **Alex Teghipco:** Writing – original draft, Visualization, Validation, Methodology, Investigation. **Chris Rorden:** Writing – review & editing, Validation, Formal analysis, Data curation. **Julius Fridriksson:** Writing – review & editing, Funding acquisition. **Mathew Chaves:** Visualization, Data curation. **Argye E. Hillis:** Writing – original draft, Investigation, Funding acquisition, Formal analysis, Data curation, Conceptualization.

Declaration of competing interest

The authors declare that they have no known competing financial interests or personal relationships that could have appeared to influence the work reported in this paper.

Data availability

Data will be made available on request.

References

Aas, K., Jullum, M., Løland, A., 2021. Explaining individual predictions when features are dependent: More accurate approximations to Shapley values. *Artif. Intell.* 298, 103502.
Cheng, B., Chen, J., Königsberg, A., et al., 2023. Mapping the deficit dimension structure of the National Institutes of Health Stroke Scale. *EBioMedicine* 87, 104425.
Christensen, S., Amukotuwa, S., Lansberg, M.G., et al., 2021. Comparison of Tmax values between full- and half-dose gadolinium perfusion studies. *J. Cereb. Blood. Flow. Metab.* 41, 336–341.
Croquelois, A., Wintermark, M., Reichhart, M., et al., 2003. Aphasia in hyperacute stroke: language follows brain penumbra dynamics. *Ann. Neurol.* 54, 321–329.
Ding, L., Liu, H., Jing, J., et al., 2023. Lesion Network Mapping for Neurological Deficit in Acute Ischemic Stroke. *Ann. Neurol.* 94 (3), 572–584. https://doi.org/10.1002/ana.26721.
Franses, P.H., 2016. A note on the Mean Absolute Scaled Error. *Int. J. Forecast.* 32, 20–22.
Hardin, D., Tsamardinos, I., Aliferis, C.F., 2004. A theoretical characterization of linear SVM-based feature selection. In: *Twenty-First International Conference on Machine Learning - ICML '04*. ACM Press, New York, New York, USA, p. 48.
Hastie, T., Tibshirani, R., Friedman, J., 2009. .. In: *The Elements of Statistical Learning*. Springer New York, New York, NY. https://doi.org/10.1007/978-0-387-84858-7.
Hillis, A.E., Kane, A., Barker, P., et al., 2001. Neural substrates of the cognitive processes underlying reading: Evidence from magnetic resonance perfusion imaging in hyperacute stroke. *Aphasiology* 15, 919–931.
Hillis, A.E., Wityk, R.J., Tuffiash, E., et al., 2001. Hypoperfusion of Wernicke's area predicts severity of semantic deficit in acute stroke. *Ann. Neurol.* 50, 561–566.
Hillis, A.E., Wityk, R.J., Barker, P.B., et al., 2002. Subcortical aphasia and neglect in acute stroke: the role of cortical hypoperfusion. *Brain* 125, 1094–1104.

Hillis, A.E., Wityk, R.J., Barker, P.B., et al., 2003. Neural regions essential for writing verbs. *Nat. Neurosci.* 6, 19–20.
Hillis, A.E., Work, M., Barker, P.B., et al., 2004. Re-examining the brain regions crucial for orchestrating speech articulation. *Brain* 127, 1479–1487.
Hillis, A.E., Newhart, M., Heidler, J., et al., 2005. Anatomy of spatial attention: insights from perfusion imaging and hemispatial neglect in acute stroke. *J. Neurosci.* 25, 3161–3167.
Hillis, A.E., Kleinman, J.T., Newhart, M., et al., 2006. Restoring Cerebral Blood Flow Reveals Neural Regions Critical for Naming. *J. Neurosci.* 26, 8069–8073.
Lyden, P., Lu, M., Jackson, C., et al., 1999. Underlying structure of the National Institutes of Health Stroke Scale: results of a factor analysis. NINDS tPA Stroke Trial Investigators. *Stroke* 30, 2347–2354.
Mah, Y.-H., Husain, M., Rees, G., et al., 2014. Human brain lesion-deficit inference remapped. *Brain* 137, 2522–2531.
Meinshausen, N., Bühlmann, P., 2010. Stability Selection. *J. R. Stat. Soc. Series. B Stat. Methodol.* 72, 417–473.
Menezes, N.M., Ay, H., Wang Zhu, M., et al., 2007. The Real Estate Factor. *Stroke* 38, 194–197.
Mwangi, B., Tian, T.S., Soares, J.C., 2014. A Review of Feature Reduction Techniques in Neuroimaging. *Neuroinformatics* 12, 229–244.
Ochfeld, E., Newhart, M., Molitoris, J., et al., 2010. Ischemia in broca area is associated with broca aphasia more reliably in acute than in chronic stroke. *Stroke* 41, 325–330.
Olsen, T.S., Larsen, B., Herning, M., et al., 1983. Blood flow and vascular reactivity in collaterally perfused brain tissue. Evidence of an ischemic penumbra in patients with acute stroke. *Stroke* 14 (3), 332–341. https://doi.org/10.1161/01.str.14.3.332.
Rajashekar, D., Wilms, M., MacDonald, M.E., et al., 2022. Lesion-symptom mapping with NIHSS sub-scores in ischemic stroke patients. *Stroke Vasc. Neurol.* 7, 124–131.
Teghipco, A., Kim, H., Rorden, C., et al., xxxx. Excellence is a habit: Enhancing predictions of language impairment by identifying stable features in clinical perfusion scans. *MedRxiv*.
Teghipco, A., Newman-Norlund, R., Gibson, M., et al., 2024. Stable multivariate lesion symptom mapping. *Aperture Neuro* 4. https://doi.org/10.52294/001c.117311.
Wang, M., Farouki, Y., Hulscher, F., et al., 2023. Severely Hypoperfused Brain Tissue Correlates with Final Infarct Volume Despite Recanalization in DMVO Stroke. *J. Belg. Soc. Radiol.* 107, 90.
Williams, L.S., Yilmaz, E.Y., Lopez-Yunez, A.M., 2000. Retrospective assessment of initial stroke severity with the NIH Stroke Scale. *Stroke* 31, 858–862.
Zavaglia, M., Forkert, N.D., Cheng, B., et al., 2015. Mapping causal functional contributions derived from the clinical assessment of brain damage after stroke. *Neuroimage Clin.* 9, 83–94.
Zou, H., Hastie, T., 2005. Regularization and Variable Selection Via the Elastic Net. *J. R. Stat. Soc. Series B Stat. Methodol.* 67, 301–320.